Supplementary Material for 'Impact resetting of the U-Pb, Pb-Pb, and Rb-Sr chronometers in the 4.3 Gyr-old lunar granitoids'

J. F. Pernet-Fisher, J. F. Snape, F. Boschetty, K. H. Joy, M. E. Hartley, D. A. Neave,

M. J. Whitehouse, R. Tartèse

(2026). *Advances in Geochemistry and Cosmochemistry*, 2(1), 771.
https://doi.org/10.33063/agc.v2i1.771

This file contains:

Supplementary Text:

Supporting Tables S1 to S13 are available from Pernet-Fisher (2025):
https://doi.org/10.48420/29126819.

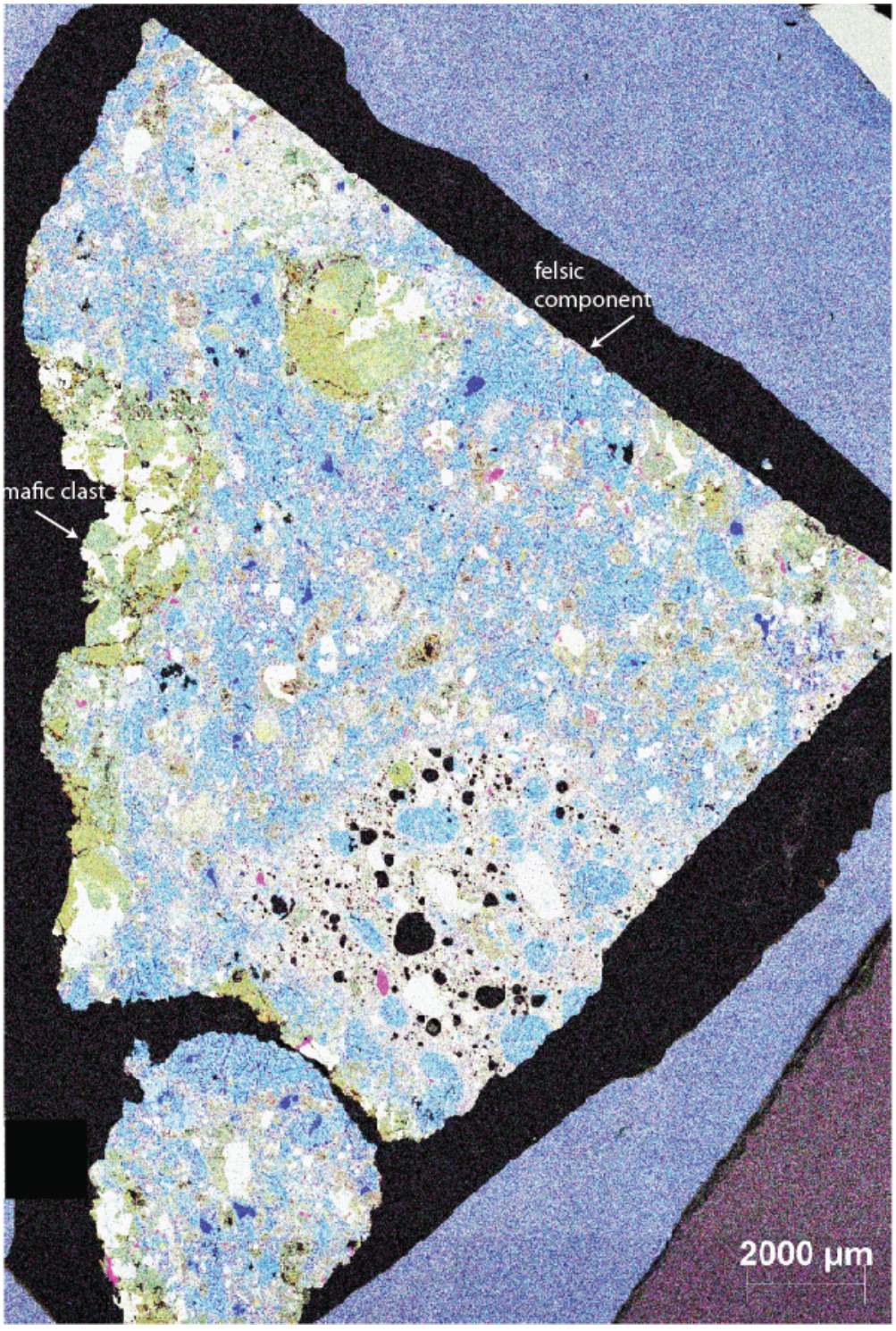

Fig. S1: False colour EDS element maps of section 12013,9. Colour scheme: Mg=green, Al=white, Si=blue, K=cyan, Ca = yellow, Ti = pink and Fe = red

S1. Rb/Sr and Pb-Pb secondary standards

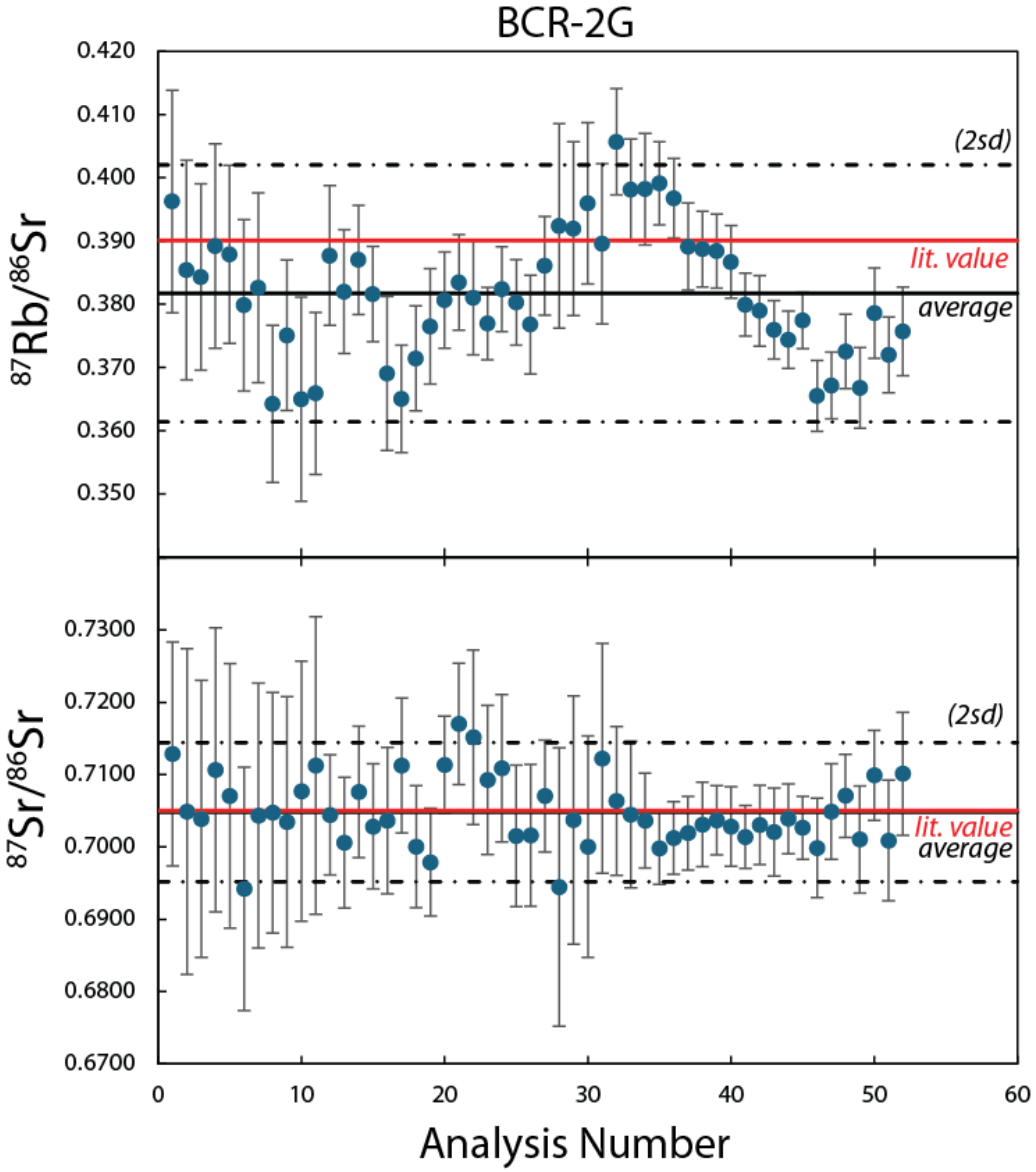

Fig S2: *In situ* Rb-Sr isotope data for basaltic glass BCR-2G across multiple analytical sessions. Black line represents the average value (dashed black line represents the 2sd uncertainties), and the red line represents the literature values (from the GeoReM database). Data are reported in **Table S6**.

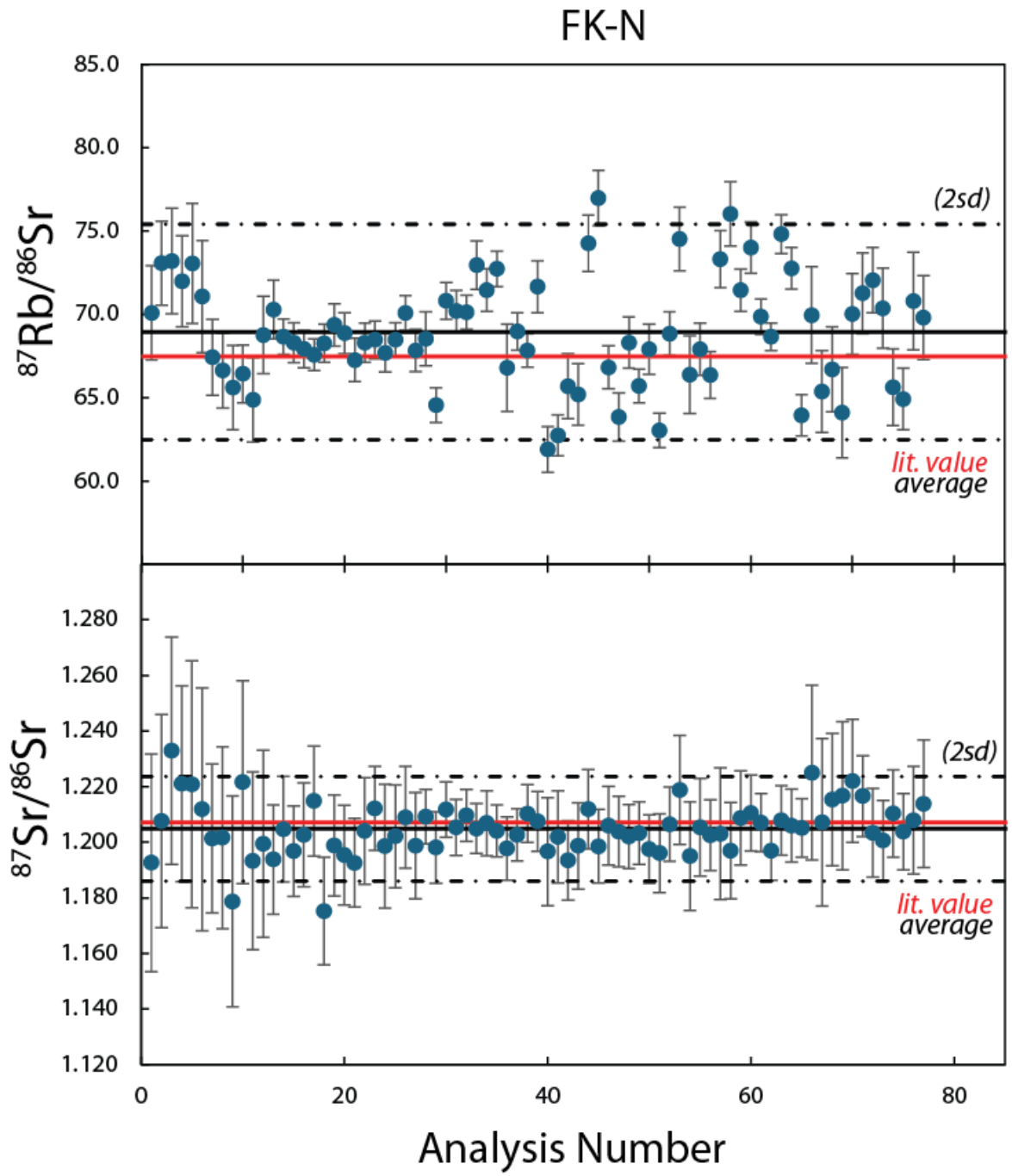

Fig S3: *In situ* Rb-Sr isotope data for feldspar pressed pellet FK-N across multiple analytical sessions. Black line represents the average value (dashed black line represents the 2sd uncertainties), and the red line represents the literature values (from Beranoaguirre et al., 2019). Data are reported in **Table S6**.

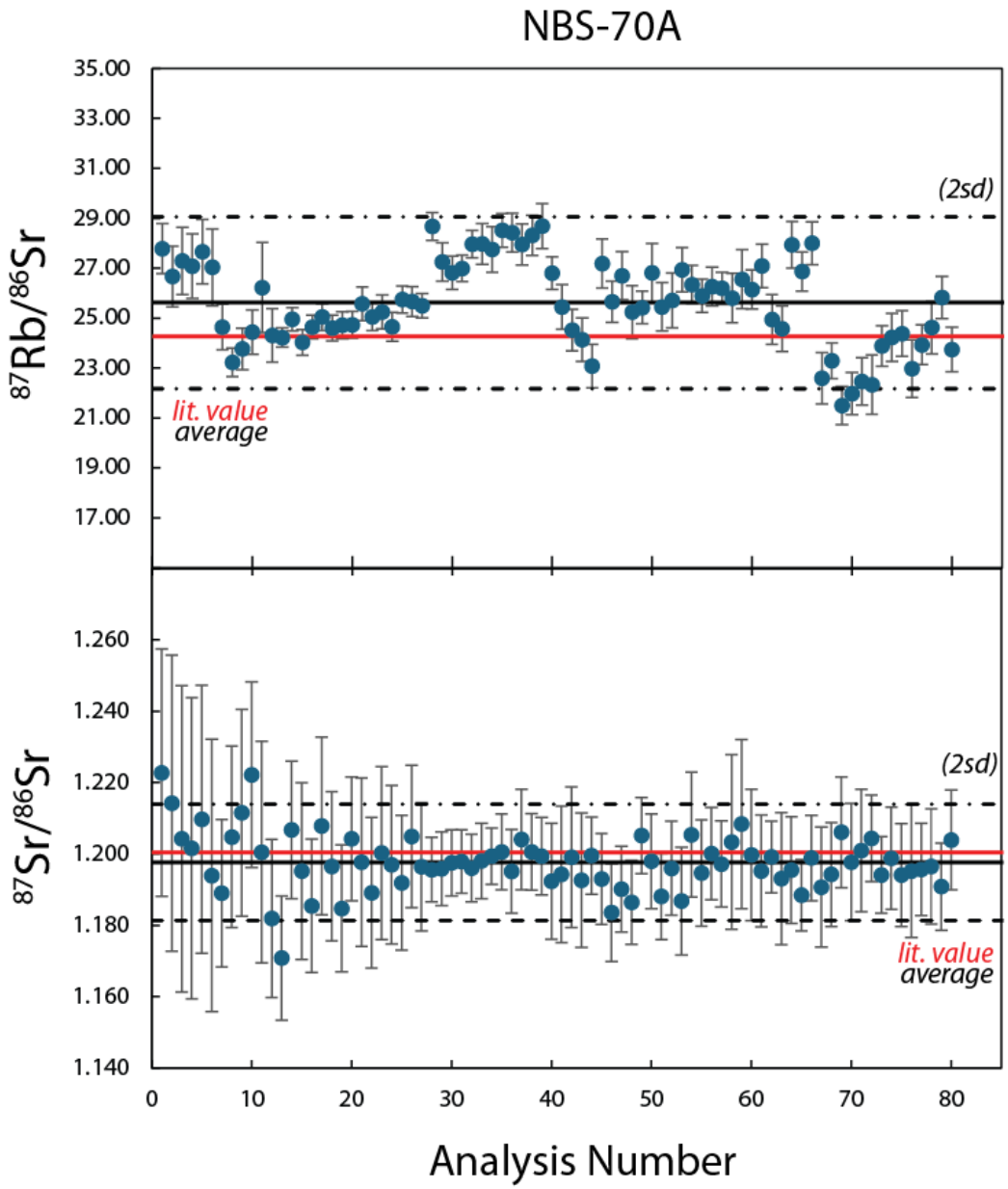

Fig S4: *In situ* Rb-Sr isotope data for feldspar pressed pellet NBS-70A across multiple analytical sessions. Black line represents the average value (dashed black line represents the 2sd uncertainties), and the red line represents the literature values (from Nebel and Mezger 2006). Data are reported in **Table S6**.

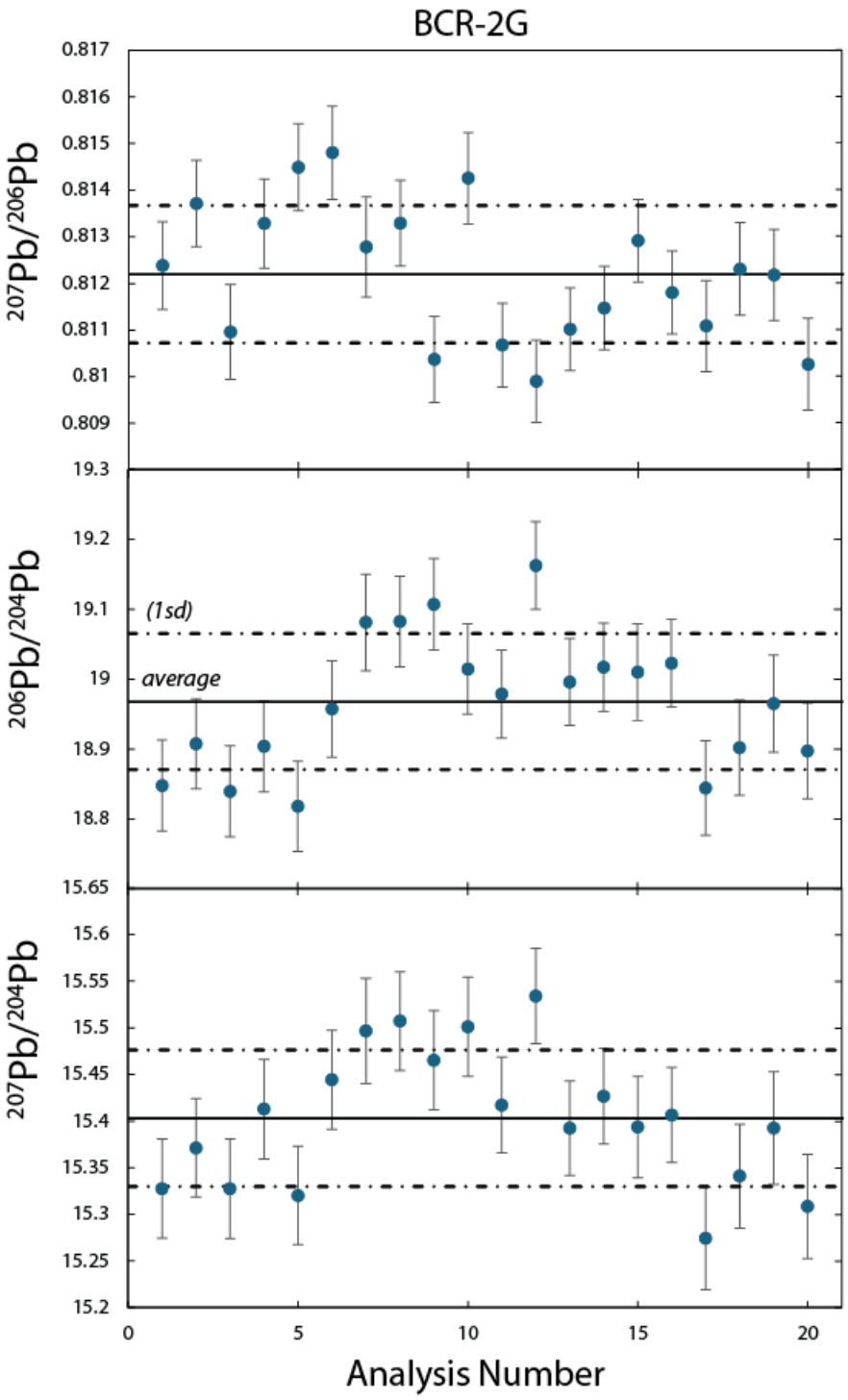

Fig. S5: *In situ* Pb isotope compositions measured by SIMS for basaltic glass BCR-2G during the analytical campaign. Black line represents the average value (dashed black line represents the 1sd uncertainties). Data in **Table S8**.

S2. Rb/Sr dating protocol validation

To validate the method for determining *in situ* Rb/Sr ages as described in section 3.2 of the main text, we analysed plagioclase and K-feldspar grains from four terrestrial granites as 'unknowns'. These samples all have well-established ages. All sample chips were mounted in epoxy and polished to produce a flat surface. The resulting *in situ* ages and initial $^{87}Sr/^{86}Sr$ ($^{87}Sr/^{86}Sr_0$), together with published TIMS values are summarised in **Fig. S6**. All errors are 2se.

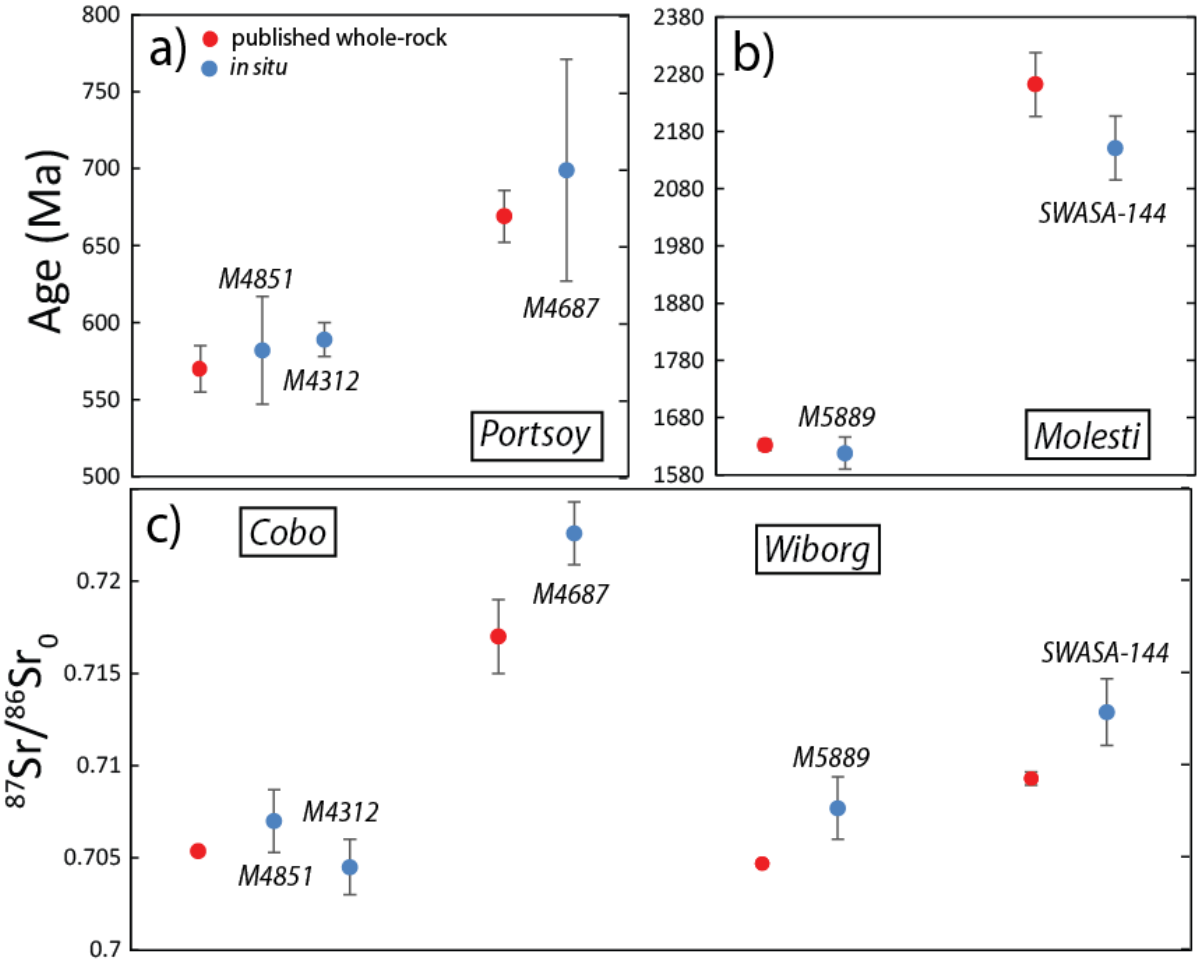

Fig. S6: a-b) Summary of *in situ* Rb-Sr ages (blue symbols) and published whole-rock Rb-Sr ages (red symbols) for the Cobo (Adams, 1976), Portsoy (Pankhurst, 1974), Wiborg (Rämö et al., 2014), and Molesti (Oliveira et al., 2025) granites. c) Summary of the initial $^{87}Sr/^{86}Sr$ values for the *in situ* (blue symbols) and published whole rock (red symbols) Rb-Sr isochrons.

S2.1 Cobo Granite, Guernsey

This pluton has a reported whole rock Rb/Sr age of 570 ± 15 Ma and an initial $^{87}Sr/^{86}Sr$ of 0.70535 ± 0.00017 (Adams 1976). Two samples (M4312 and M4851) were acquired from the Manchester Museum geological collection. Using the *in situ* Rb/Sr protocol reported here, we obtained ages of 582 ± 35 Ma and 589 ± 11 Ma, respectively (**Fig. S7** and **Table S7**).

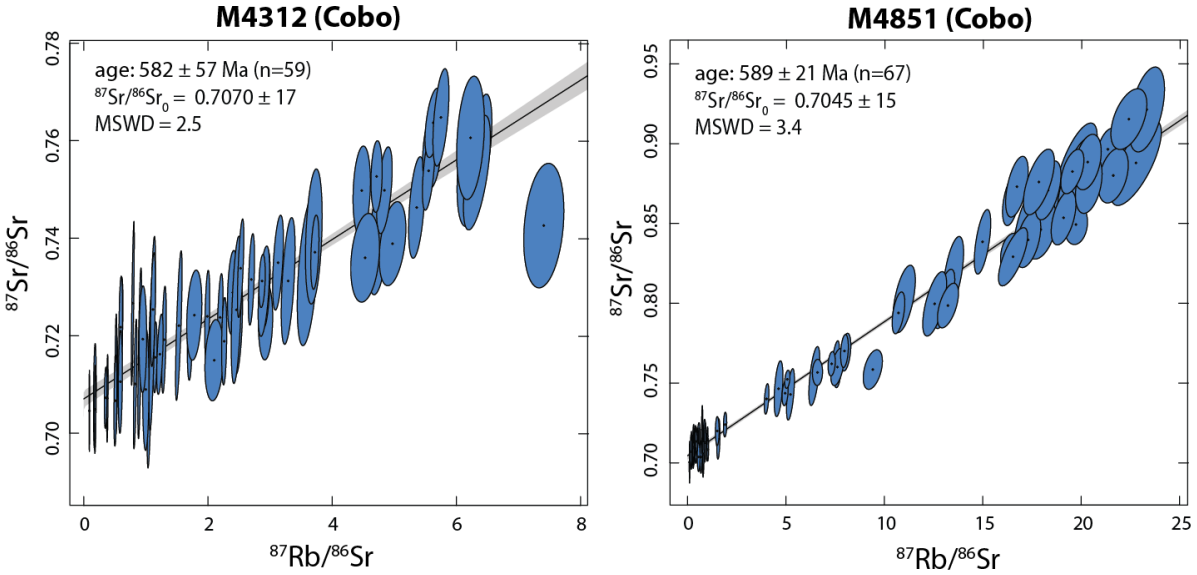

Fig. S7: Plagioclase and K-feldspar Rb-Sr isochrons for 2 samples (M4312 and M4851) from the Cobo granite. Blue ellipses represent 2se errors.

S2.2 Portsoy Granite, Scotland

This pluton has a reported whole rock Rb/Sr age of 667 ± 17 Ma and an initial $^{87}Sr/^{86}Sr$ of 0.7170 ± 0.0020 (Pankhurst, 1974). Sample M4687 was acquired from the Manchester Museum geological collection. We determined an *in situ* age of 699 ± 72 Ma (**Fig. S8** and **Table S7**). The large error in our reported age reflects the small range of $^{87}Rb/^{86}Sr$ values measured from the single section analysed.

S2.3 Wiborg Granite, Finland

This pluton has a reported whole rock Rb/Sr age of 1632 ± 10 Ma and an initial $^{87}Sr/^{86}Sr$ of 0.70470 ± 0.00005 (Rämö et al., 2014). Sample M5889 was acquired from the Manchester

Museum geological collection. We obtained an *in situ* age of 1620 ± 24 Ma (**Fig. S8** and **Table S7**).

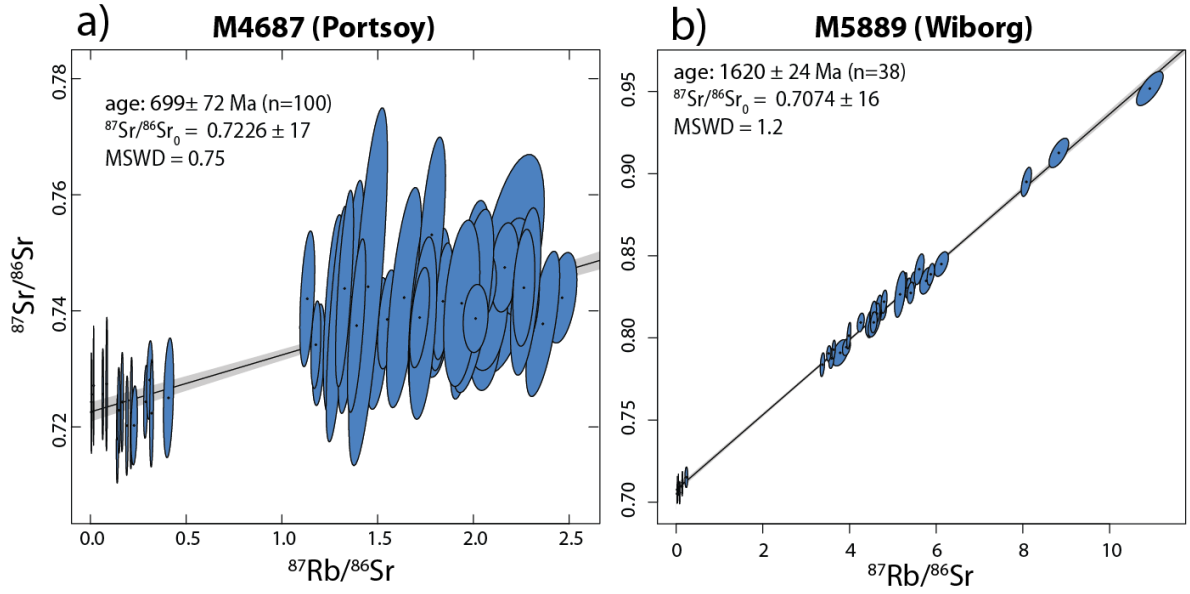

Fig. S8: a) Plagioclase and K-feldspar Rb-Sr isochron for sample M4687 from the Portsoy Granite. Blue ellipses represent 2se errors. b) Plagioclase and K-feldspar Rb-Sr isochron for sample M5889 from the Wiborg Granite. Blue ellipses represent 2se errors.

S2.4 Molesti Pluton, Zimbabwe

Solution ICP-MS and TIMS analyses (for Rb and Sr abundances, and $^{87}Sr/^{86}Sr$ values, respectively) were measured on plagioclase and K-feldspar mineral separates from a sub-sample of SWASA-144 on loan to the University of Manchester. These analyses yielded an age of 2262 ± 56 Ma, with an initial $^{87}Sr/^{86}Sr$ ratio of 0.70930 ± 0.00035 (Oliveira et al., 2025). From the same sub-sample, we mounted and polished a chip in epoxy for *in situ* analysis. Across 3 sessions our *in situ* Rb-Sr isotopes analyses of plagioclase and K-feldspar yields an age of 2151 ± 65 Ma (**Fig. S10a** and **Table S7**). Individual ages for each session are plotted in **Fig. S10b**. Our average date across these sessions are consistent with published TIMS ages.

Notably, the Molesti pluton has a complex thermal history which is reflected by the range of ages reported for this pluton in the literature. Reported U-Pb zircon ages from this pluton indicate a crystallisation age of ~2.69 Ga (Laurent et al., 2013). By contrast, a biotite-whole rock Rb-Sr from this pluton reported by Barton and Van Reenen (1992) yields an age of 2128 ± 15 Ma. This younger age is consistent with to other biotite-while rock Rb-Sr ages from

plutons within the central and southern marginal zones of the Limpopo Belt and has been linked to a period of thermal disturbance due to regional crustal uplift (Barton and Van Reenen, 1992).

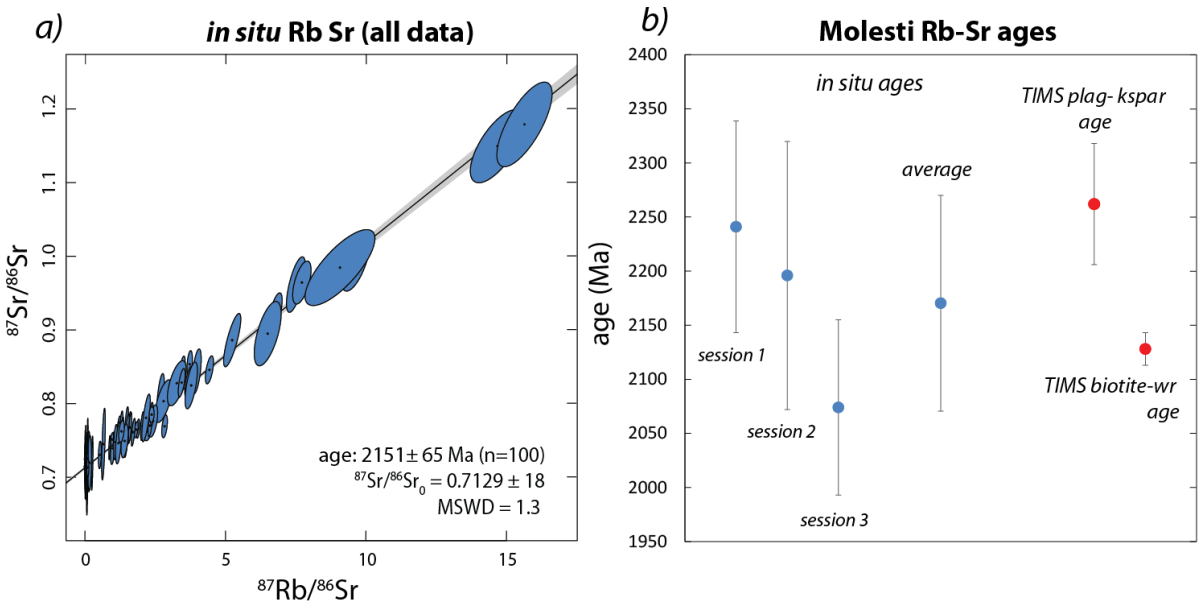

Fig. S10: a) Plagioclase and K-feldspar Rb-Sr isochron for sample SWASA-144 from the Molesti pluton. Data plotted is from three separate analytical sessions. Blue ellipses represent 2se errors. b) Summary of *in situ* Rb-Sr ages (blue symbols) and published TIMS Rb-Sr ages (red symbols). The TIMS plagioclase/K-feldspar age is from Oliveira et al. (2025) and the TIMS biotite-whole rock age is from Barton and Van Reenen (1992).

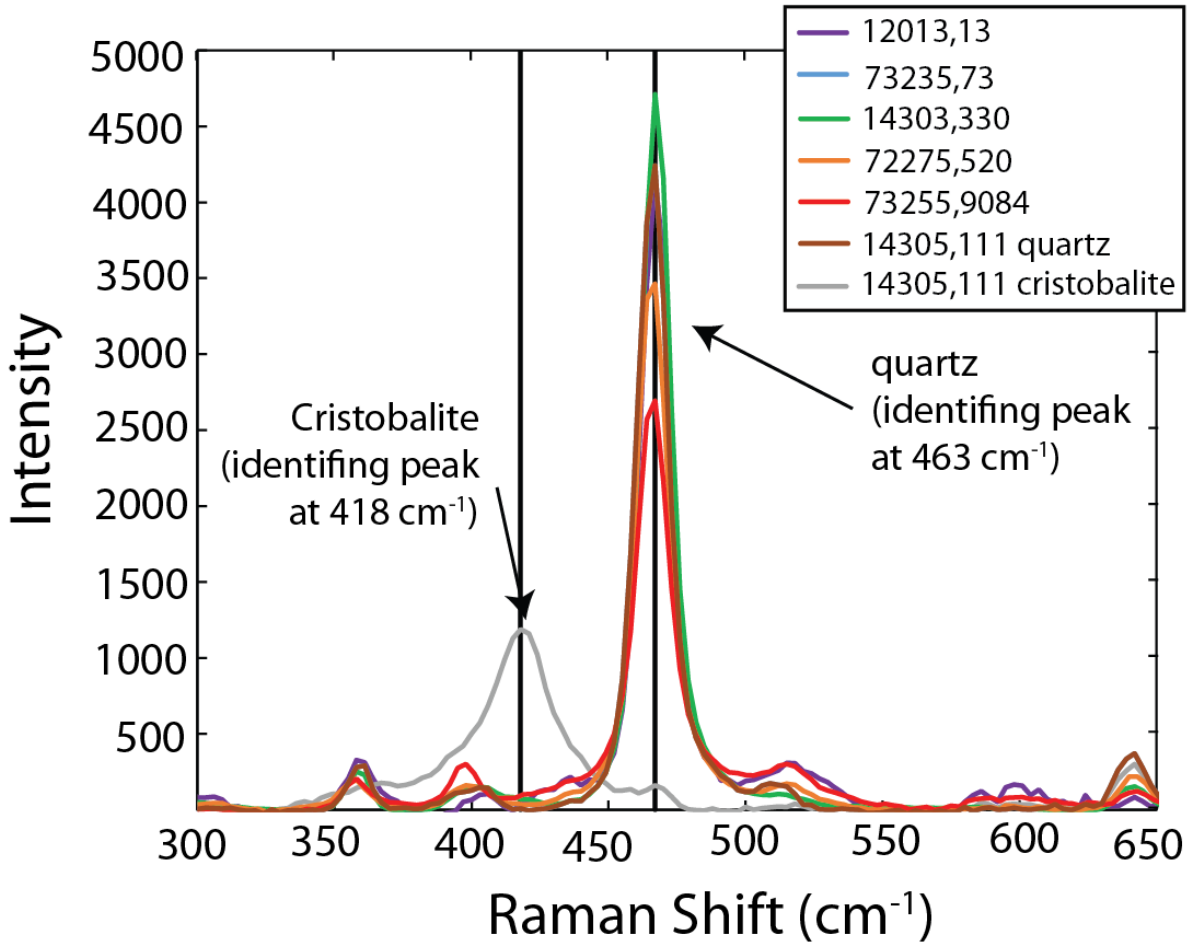

Fig. S11: Average background corrected Raman spectra of silica from Apollo granites (full data set reported in **Table S9**). Vertical black line highlights the identifying peak for 463 cm^{-1} and 418 cm^{-1} for quartz and cristobalite, respectively. Only in one sample, 14305,111, was cristobalite observed.

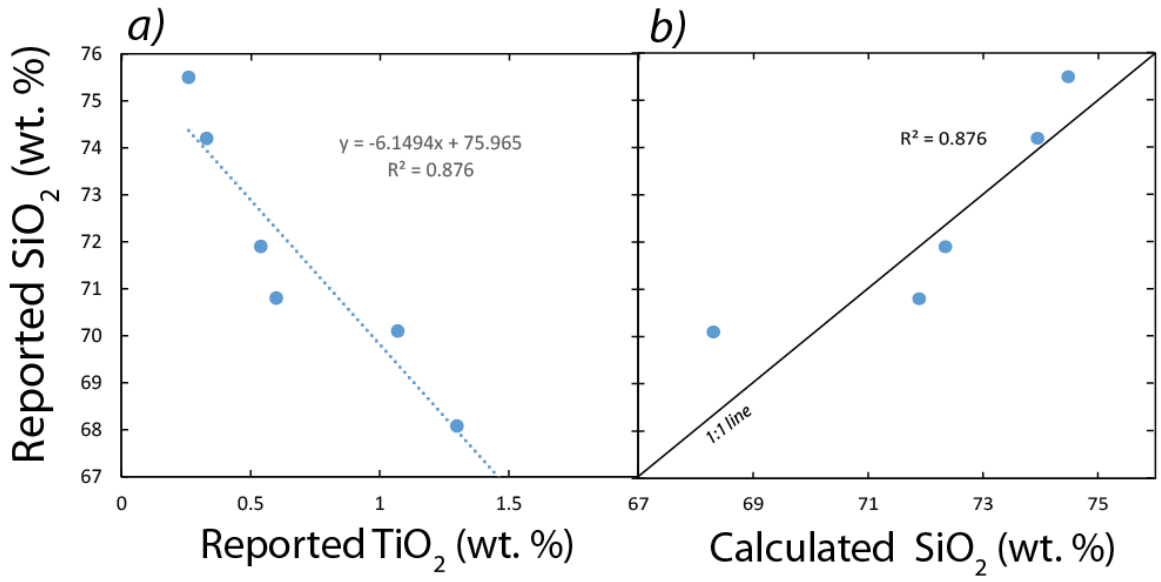

Fig. S12: a) Reported bulk-rock SiO_2 vs. bulk-rock TiO_2 (wt. %) for Apollo granites (data from Papike et al. (2008) and references therein). This correlation was used to estimate the bulk SiO_2 abundances using reported TiO_2 abundances. To test the accuracy of this method, directly measured SiO_2 values are plotted against our calculated SiO_2 values in (b) using the linear equation described in panel a).

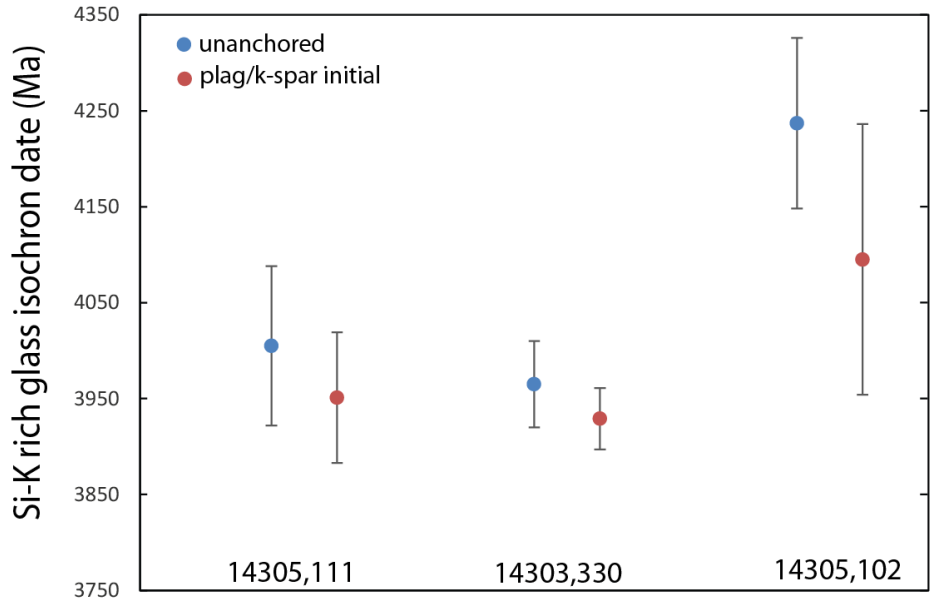

Fig. S13: Dates (Ma) for Si-K-rich glass isochrons. Blue symbols represent dates calculated using a regression that does not have the initial $^{87}Sr/^{86}Sr$ anchored to a fixed value. The red symbols represent dates calculated by anchoring the initial $^{87}Sr/^{86}Sr$ to the initial Sr-isotope ratio calculated for the plagioclase/K-feldspar isochrons.

S3: Partial melt modelling

To help constrain how trace elements fractionate during the of melting of phosphate-bearing and phosphate-free source lithologies, we calculate the composition of partial melts using the batch partial melting equation of Shaw (1979):

$C_L/C_0 = 1/[D_0 + F(1 - D_0]$

Where C_L and C_0 are the concentration of a trace element in the melt and source respectively, F is the weight fraction of the melt produced, and D_0 is the bulk distribution coefficient. D_0 is calculated from $D_0 = [D_1 * d_1] + [D_2 * d_2] + [D_3 * d_3] + \ldots$ where D_1, D_2, D_3 are mineral-melt partition coefficient and d_1, d_2, d_3 are the weight fraction of the mineral (i.e. mineral mode) in the source lithology.

The modelling presented here considers a Si-rich source lithology (representing the crystallized product of a Si-rich immiscible fraction during the formation of urKREEP) and a KREEP-rich mafic lithology representing an appropriate source lithology for the basaltic underplating model (see section 4.4 for more details).

For the Si-rich lithologies we use stating composition of 24 ppm Sm and 11 ppm Th (using terrestrial $D_{Fe\text{-}liq/Si\text{-}liq}$ values; Veksler et al., 2006) and 12 ppm Sm and 5 ppm Th (using estimated lunar $D_{Fe\text{-}liq/Si\text{-}liq}$ values; Neal and Taylor 1989). For a mafic lithologies we use the composition of KREEP basalt 15386; that has 37 ppm Sm and 14 ppm Th (Hubbard 1974).

Few mineral-melt partition coefficients (D-values) have been reported that are appropriate for felsic systems under lunar conditions (i.e., low fO_2) for, as such we use terrestrial reported mineral-melt D-values (sourced from the GERM partition coefficient database (https://kdd.earthref.org/KdD). For mineral melt D-values in a mafic system we use the D-values reported by Dygert et al. (2020). The table below summarizes the mineral-melt D-values and weight fraction (d_x) in the source lithologies used for our calculations. Note that whereas Bea et al. (1994) report apatite D values of 1105 and 41 for Sm and Th respectively for granitic systems, the GERM database indicates that D_{Sm} can extends to much lower values (84; Nagasawa (1970). No D_{Th} were reported by this study, however based on the range of D_{Th} reported by the GERM database, D_{Th} are typically an order of magnitude lower

than D_{Sm}, therefore we estimate a lower D_{Th} of 4. Mafic d_x values are a typical basalt mineral mode (e.g., Warner et al 1975; Cousin et al., 2012). Felsic d_x values reflect the mineral modes observed in the evolved lithologies studied here.

Table S14: Mineral-melt *D* values and d_x fractions used in the partial melt modelling presented here.

	D_{Sm}	D_{Th}	Reference		d_x
Felsic melts					
Plagioclase	0.11 to 0.23	0.03 to 0.08	Nash and Crecraft (1985)		0.450
K-feldspar	0.02 to 0.04	0.02 to 0.03	Nash and Crecraft (1985)		0.400
SiO_2	<0.0001	<0.0001	No values reported		0.145
Mafic Melts					
Olivine	0.0002	0.0001	Dygert et al. (2020)		0.250
Pyroxene	0.04	0.0011	Dygert et al. (2020)		0.600
Plagioclase	0.001	0.01	Dygert et al. (2020)		0.145
Phosphates					0.005
Apatite	84 to 1105	~4 to 41	Bea et al. (1994)		
Merrillite	26	1.4	Ludberg et al., (1990); Benjamin et al. (1978)		

S4: High Precision Ti in silica:

Using the silicate EPMA routine detailed in section 3.2 of the main text, the detection limits for Ti in silica are~ 300 ppm. For silica grains in NWA 4472, we also them using a Cameca SX100 EPMA at the University of Manchester following the method outlined by Donovan et al. (2011). This method achieved detection limits of 2.4 ppm.

Analyses were carried out using a 25 kV accelerating voltage, a 60 nA beam current, and a defocused 5 μm beam size. Measurements were made using LPET and PET spectrometers. Rutile was used to identify the position of the TiO_2 peak and backgrounds positions. Spectrosil glass (pure SiO_2) was used a Ti-free reference material. Counting times for each spectrometer was 480 s on peak and 480 s off peak. All data is reported in **Table S13**.

.

References:

Adams, C. J. D. (1976). Geochronology of the Channel Islands and adjacent French mainland. Journal of the Geological Society, 132(3), 233–250. https://doi.org/10.1144/gsjgs.132.3.0233

Bea, F., Pereira, M. D., & Stroh, A. (1994). Mineral/leucosome trace-element partitioning in a peraluminous migmatite (a laser ablation-ICP-MS study). Chemical Geology, 117, 291-312. https://doi.org/10.1016/0009-2541(94)90133-3

Beranoaguirre, A., Pin, C., Sanchez-Lorda, M. E., de Madinabeitia, S. G., & Gil Ibarguchi, J. I. (2019). An evaluation of Rb-Sr isotope dilution analyses with a 86Sr-enriched tracer and Multiple Collection-ICP-MS. International Journal of Mass Spectrometry, 435, 234-240. https://doi.org/10.1016/j.ijms.2018.10.035

Barton Jr, J. M., & Van Reenen, D. D. (1992). When was the Limpopo orogeny? Precambrian Research, 55, 7-16. https://doi.org/10.1016/0301-9268(92)90010-L

Benjamin, T. M., Heuser, W. R., & Burnett, D. S. (1978). Laboratory studies of actinide partitioning relevant to 244 Pu chronometry. In Proceedings of the 9th Lunar and Planetary Science Conference, 9, 1393-1406.

Cousin, A., Sautter, V., Fabre, C., Maurice, S., & Wiens, R. C. (2012). Textural and modal analyses of picritic basalts with ChemCam laser-induced breakdown spectroscopy. Journal of Geophysical Research: Planets, 117(E10). https://doi.org/10.1029/2012je004132

Dygert, N., Draper, D. S., Rapp, J. F., Lapen, T. J., Fagan, A. L., & Neal, C. R. (2020). Experimental determinations of trace element partitioning between plagioclase, pigeonite, olivine, and lunar basaltic melts and an fO2 dependent model for plagioclase-melt Eu partitioning. Geochimica et Cosmochimica Acta, 279, 258-280. https://doi.org/10.1016/j.gca.2020.03.037

Donovan, J. J., Lowers, H. A., & Rusk, B. G. (2011). Improved electron probe microanalysis of trace elements in quartz. American Mineralogist, 96, 274-282. https://doi.org/10.2138/am.2011.3631

Hubbard, N. J., Rhodes, J. M., Wiesmann, H., Shih, C. Y., & Bansal, B. M. (1974). The chemical definition and interpretation of rock types returned from the non-mare regions of the moon. In Proceedings of the 5th Lunar and Planetary Science Conference, 5, 1227-1246.

Laurent, O., Paquette, J. L., Martin, H., Doucelance, R., & Moyen, J. F. (2013). LA-ICP-MS dating of zircons from Meso- and Neoarchean granitoids of the Pietersburg block (South Africa): crustal evolution at the northern margin of the Kaapvaal craton. Precambrian Research, 230, 209-226. https://doi.org/10.1016/j.precamres.2013.02.009

Lundberg, L. L., Crozaz, G., & McSween Jr, H. Y. (1990). Rare earth elements in minerals of the ALHA77005 shergottite and implications for its parent magma and crystallization history.

Geochimica et Cosmochimica Acta, 54, 2535-2547. https://doi.org/10.1016/0016-7037(90)90240-L

Moyen, J. F., McCoy-West, A. J., Bruand, E., Millet, M. A., Nebel, O., Cawood, P. A., Saji, N., Ladwig, A., Klaver, M., & Elburg, M. (2024). Felsic crust development in the Kaapvaal Craton, South Africa: A reference sample collection to investigate a billion years of geological history. Earth-Science Reviews, 250, 104680. https://doi.org/10.1016/j.earscirev.2024.104680

Nebel, O., & Mezger, K. (2006). Reassessment of the NBS SRM-607 K-feldspar as a high precision Rb/Sr and Sr isotope reference. Chemical Geology, 233, 337-345. https://doi.org/10.1016/j.chemgeo.2006.03.003

Neal, C. R., & Taylor, L. A. (1989). The nature and barium partitioning between immiscible melts-A comparison of experimental and natural systems with reference to lunar granite petrogenesis. In 19th Lunar and Planetary Science Conference, 19, 209-218.

Nagasawa, H. (1970). Rare earth concentrations in zircons and apatites and their host dacites and granites. Earth and Planetary Science Letters, 9, 359-364. https://doi.org/10.1016/0012-821x(70)90136-6

Nash, W. P., & Crecraft, H. R. (1985). Partition coefficients for trace elements in silicic magmas. Geochimica et Cosmochimica Acta, 49, 2309-2322. https://doi.org/10.1016/0016-7037(85)90231-5

Oliveira, B. H., Snape, J. F., Tartèse, R., Pernet-Fisher, J. F., van Acken, D., Whitehouse, M. J., & Joy, K. H. (2025). Insights on the volcanic and impact histories of the lunar nearside from the petrology, geochemistry, and geochronology of the Calcalong Creek lunar regolith breccia meteorite. Meteoritics & Planetary Science. https://doi.org/10.1111/maps.14305

Pankhurst, R. J. (1974). Rb-Sr whole-rock chronology of Caledonian events in northeast Scotland. Geological Society of America Bulletin, 85, 345-350. https://doi.org/10.1130/0016-7606(1974)85<345:rwcoce>2.0.co;2

Papike, J. J., Ryder, G., & Shearer, C. K. (1998). Lunar samples. Planetary materials, 36, 1-234. https://doi.org/10.1515/9781501508806-020

Rämö, O. T., Turkki, V., Mänttäri, I., Heinonen, A., Larjamo, K., & Lahaye, Y. (2014). Age and isotopic fingerprints of some plutonic rocks in the Wiborg rapakivi granite batholith with special reference to the dark wiborgite of the Ristisaari Island. Bulletin of the Geological Society of Finland, 86, 71-91. https://doi.org/10.17741/bgsf/86.2.002

Shaw, D. M. (1979). Trace element melting models. Physics and Chemistry of the Earth, 11, 577-586. https://doi.org/10.1016/0079-1946(79)90055-7

Veksler, I. V., Dorfman, A. M., Danyushevsky, L. V., Jakobsen, J. K., & Dingwell, D. B. (2006). Immiscible silicate liquid partition coefficients: implications for crystal-melt element

partitioning and basalt petrogenesis. Contributions to Mineralogy and Petrology, 152, 685-702. https://doi.org/10.1007/s00410-006-0127-y

Warner, J. (1975). Mineralogy, petrology, and geochemistry of the lunar samples. Reviews of Geophysics, 13, 107-113. https://doi.org/10.1029/rg013i003p00107